

Multispectral image denoising by well-posed anisotropic diffusion scheme with channel coupling

V. B. SURYA PRASATH and ARINDAMA SINGH*

Department of Mathematics, Indian Institute of Technology Madras,
Chennai 600036, India

(Received 3 June 2009; in final form 12 August 2009)

A novel way to denoise multispectral images is proposed via an anisotropic diffusion based partial differential equation (PDE). A coupling term is added to the divergence term and it facilitates the modelling of interchannel relations in multidimensional image data. A total variation function is used to model the intrachannel smoothing and gives a piecewise smooth result with edge preservation. The coupling term uses weights computed from different bands of the input image and balances the interchannel information in the diffusion process. It aligns edges from different channels and stops the diffusion transfer using the weights. Well-posedness of the PDE is proved in the space of bounded variation functions. Comparison with the previous approaches is provided to demonstrate the advantages of the proposed scheme. The simulation results show that the proposed scheme effectively removes noise and preserves the main features of multispectral image data by taking channel coupling into consideration.

1. Introduction

Multispectral images are acquired using multiple frequency bands and contain useful information which is otherwise not captured by optical cameras. Denoising such images is paramount to distinguishing important features from noise (Acton and Landis 1997, Pope and Acton 1998, Lennon *et al.* 2002, Smolka and Lukac 2002, Wang *et al.* 2005) and aids further processes like segmentation (Karantzalos and Argialas 2006, Im *et al.* 2008). Regularization methods (Tschumperlé and Deriche 2005) and partial differential equations (PDEs) (Perona and Malik 1990, Rudin *et al.* 1992, Aubert and Kornprobst 2006) are widely employed in denoising images and are good at stabilizing restoration which is, in general, ill-posed. In the case of multispectral images, due to the existence of non-trivial correlations between different bands, channel-wise application of these schemes often fail and remove significant features along with noise.

Colour images can be considered as a special case of multispectral images with three channels, namely red, green and blue (R,G,B). In recent times there have been efforts to use the powerful diffusion PDE paradigm in denoising such colour images (Boccignone *et al.* 2002, Tschumperlé and Deriche 2005, Aubert and Kornprobst 2006). With respect to multispectral images, Acton and Landis (1997) used dissimilarity measures computed using all the channels inside the diffusion term to capture correlations. Other similar diffusion based schemes have been studied since then (see

*Corresponding author. Email: asingh@iitm.ac.in

Pope and Acton (1998), Lennon *et al.* (2002), Smolka and Lukac (2002), Wang *et al.* (2005)). These methods are based on the original formulation of Perona and Malik (1990) and induce smearing of edges and oversmoothing of flat regions. Boccignone *et al.* (2002) introduce a coupling term to capture chromatic edges utilizing the diffusion PDE with Laplacian as an intrachannel term. This results in colour smearing near chromatic edges as Laplacian based smoothing is isotropic in nature. Tschumperlé and Deriche (2005) integrated all the diffusion models into one common framework. To model the interchannel relations in an efficient and explicit way, in this paper, we make use of a correlation term along with an anisotropic intrachannel diffusion term. By penalizing the large differences between gradients among different bands, the proposed scheme overcomes the drawbacks of other schemes. The proposed scheme is a variant of the Perona–Malik Diffusion PDE (Perona and Malik 1990) with total variation (Rudin *et al.* 1992, Bresson and Chan 2008) diffusion function for effective intrachannel edge preservation. The correlation term effectively combines the main features and salient edges using gradient information from all the bands. We prove the well-posedness of the PDE in the bounded variation space (Giusti 1984) which is well suited to handle images. Comparisons with related diffusion schemes on multispectral data show that incorporating cross-channel correlations greatly improves the denoising performance and preserves edges.

Here we limit ourselves to multispectral images which are made up of a discrete number of bands, in contrast to hyperspectral images. Though the proposed scheme can be extended to such hyperspectral images, introducing diffusion transfer along the spectral axis needs to be addressed carefully; see Martín-Herrero (2007). Indeed, as discussed in detail by Martín-Herrero (2007), hyperspectral images have implicit correlations between adjacent channels; hence, diffusion among different bands is an important factor in noise removal.

The rest of the paper is organized as follows. In § 2 we introduce the diffusion PDE based scheme and prove the well-posedness in $BV(\Omega; \mathbb{R}^N)$. In § 3 we discuss the numerical results and present comparison with other related schemes. Finally, § 4 concludes the paper.

2. Diffusion PDE

Let $\mathbf{u} : \Omega \subset \mathbb{R}^2 \rightarrow \mathbb{R}^N$ denote the multispectral image with N bands, $\mathbf{u} = (u^1, \dots, u^N)$ where Ω is the image domain. Consider the multidimensional version of the Perona–Malik diffusion PDE (Perona and Malik 1990), for $i = 1, 2, \dots, N$ and $x \in \Omega$,

$$\frac{\partial u^i}{\partial t} = \operatorname{div} (g(|\nabla u^i|) \nabla u^i) \quad \text{with } u^i(x, 0) = u_0^i(x) \quad (1)$$

where $g : [0, \infty) \rightarrow [0, \infty)$ is a diffusion coefficient function and $u_0 = (u_0^1, \dots, u_0^N)$ is the noisy input image. The variable time t is considered as a parameter and we get a series of denoised images starting from the initial noisy image at $t = 0$. Perona and Malik's original choices for the function g are $g(s) = \exp(-s^2/K)$ and $g(s) = (1 + s^2/K)^{-1}$, where K is the contrast parameter. The channel-wise approach using (1) ignores the interchannel correlations present in the multispectral images. Thus edges specific to one band or one image plane are diffused and merged in the final output. To avoid this we propose to use the following coupled PDE:

$$\frac{\partial u^i}{\partial t} = \operatorname{div}(g(|\nabla u^i|)\nabla u^i) + \alpha \sum_{j=1}^N (\omega^i \Delta u^j - \omega^j \Delta u^i) \quad (2)$$

for $i = 1, 2, \dots, N$. The second term on the right hand side in equation (2) models the interchannel relations and balances the diffusion induced by this term and the Perona–Malik type divergence term. The adaptive weights are chosen as follows

$$\omega^i = \nabla_{\rho} u_0^i = G_{\rho} \star \nabla u_0^i \quad (3)$$

where \star denotes the convolution, and a Gaussian kernel $G_{\rho} = (2\pi\rho)^{-1} \exp(-|x|^2/2\rho)$ is used to smooth the initial noisy image. Notice that increasing the smoothing parameter ρ in equation (3) keeps only large scale edges from other channels and results in losing small scale details in the final denoised image. After performing extensive numerical experiments we found that when the noise variance is low to medium ($10 \leq \sigma \leq 20$), setting $\rho = 2$ gives a satisfactory result. We incorporate the edges of different channels via a smoothed gradient to control the denoising near discontinuities. We make use of the total variation (TV) diffusion function $g(s) = s^{-1}$, due to its better edge preservation property (Rudin *et al.* 1992) over other diffusion functions. Next, we prove the well-posedness of the proposed PDE.

THEOREM *Let $\mathbf{u}(x, 0) = \mathbf{u}_0(x) \in BV(\Omega; \mathbb{R}^N)$ be the initial image. Then the PDE (2) has a unique solution $\mathbf{u} \in BV(\Omega; \mathbb{R}^N)$.*

Proof Let $\mathcal{A}^i := -\operatorname{div}(g(|\nabla u^i|)\nabla u^i) - \alpha \sum_{j=1}^N (\omega^i \Delta u^j - \omega^j \Delta u^i)$. Here, \mathcal{A}^i is the sub-differential of the regularization functional $E^i : L^2(\Omega; \mathbb{R}^N) \rightarrow \mathbb{R}$ given by

$$E^i(u) = \int_{\Omega} \phi(|\nabla u^i(x)|) dx + \alpha \sum_{j=1}^N \int_{\Omega} (\omega^i \nabla u^j(x) - \omega^j \nabla u^i(x))^2 dx \quad (4)$$

if $\mathbf{u} \in W^{1,1}(\Omega; \mathbb{R}^N)$ with $\phi'(s) = sg(s)$ and $E^i(u) = +\infty$ if $\mathbf{u} \in L^2(\Omega; \mathbb{R}^N) \setminus W^{1,1}(\Omega; \mathbb{R}^N)$. Consider the following relaxed functional on $BV(\Omega; \mathbb{R}^N)$:

$$\tilde{E}^i(\mathbf{u}) = \int_{\Omega} \phi(|\nabla u^i(x)|) dx + \alpha \sum_{j=1}^N \int_{\Omega} (\omega^i \nabla u^j(x) - \omega^j \nabla u^i(x))^2 dx + c|\nabla_s u|$$

with $\nabla_s u$ as the singular part, $c = \lim_{t \rightarrow \infty} \phi(t)/t$, and $\tilde{E}^i(\mathbf{u}) = +\infty$ if $\mathbf{u} \in L^2(\Omega; \mathbb{R}^N) \setminus BV(\Omega; \mathbb{R}^N)$. Now, ϕ is strictly convex and the coupling term is a quadratic function. This implies \tilde{E}^i is lower semicontinuous on $BV(\Omega; \mathbb{R}^N)$, for each i , i.e. $\tilde{E}^i(\mathbf{u}) \leq \liminf_{n \rightarrow \infty} \tilde{E}^i(\mathbf{u}_n)$ for every sequence $\mathbf{u}_n \rightharpoonup \mathbf{u}$ in $BV(\Omega; \mathbb{R}^N)$. It then follows that \mathcal{A}^i is a maximal monotone operator. Using the theory of monotone operators – see Theorem 3.1 in Brezis (1973) – we conclude that the proposed PDE in equation (2) has a unique solution $\mathbf{u} = (u^1, \dots, u^N)$ in $BV(\Omega; \mathbb{R}^N)$. \square

The above existence theorem holds true for convex linear growth functions ϕ . For example, the TV function $g(s) = s^{-1}$ corresponds to the regularization function $\phi(s) = s$. The original Perona–Malik diffusion functions correspond to non-convex regularization functions and hence we cannot obtain a similar result. Since schemes such as those of Acton and Landis (1997), Pope and Acton (1998), Boccignone *et al.* (2002), Lennon *et al.* (2002), and Wang *et al.* (2005) are based on the original ill-posed Perona–Malik formulation, they remain beyond theoretical justifications.

From equation (4) we see that the proposed PDE in equation (2) is related to variational regularization schemes. We chose the divergence formulation instead of the tensor model of Tschumperlé and Deriche (2005) as we would like to incorporate interchannel correlations apart from controlling intrachannel smoothing in an edge preserving way. The above theorem, in general, can hold for any convex coupling term in (4), e.g. $\int_{\Omega} \psi(|\omega^i \nabla u^i(x) - \omega^j \nabla u^j(x)|) dx$. Our choice in equation (2) thus corresponds to setting $\psi(s) = s^2$ penalizing large deviations in gradients with guidance provided by the input image. Other choices can be used to create anisotropic coupling between different bands.

Choices regarding the interchannel weights ω^i in PDE (2) are also possible; we prefer to use the smoothed gradients as it gives a road map of discontinuities, thereby capturing meaningful edges of all the channels. Another simple choice is $\omega^i = 1$ for all $i = 1, 2, \dots, N$. In this case, the channel edges are aligned but as has been observed experimentally, the data mixing can occur between different channels due to lack of control over the edge magnitudes. In case the input signal contains high levels of noise ($\sigma > 20$), one can use the updated version \mathbf{u} (instead of \mathbf{u}_0) in the weight computation (equation 3), i.e.

$$\omega^i = \nabla_{\rho} u^i = G_{\rho} \star \nabla u^i \quad (5)$$

This enables the diffusion PDE to adapt as t increases so that the edges are preserved, and the noise removal property is increased; see §3 for an example.

3. Numerical results

For computational purposes, all the images are normalized to the range $[0, 1]$ and the implementation was carried out on a PC Pentium IV 2.40 GHz workstation with MATLAB 7.4 for visualization. The TV scheme implementation of Chambolle (2004) and the central difference approximations for the Laplacian terms in the coupling function were used.

The first example (figure 1) shows a multispectral image of the Mississippi river and surrounding farmlands obtained using the Spaceborne Imaging Radar-C/X-band Synthetic Aperture (SIR-C/X-SAR) system on October 9, 1994. The different colours represent the data acquired in different radar channels: red is L-band (24 cm), vertically transmitted and vertically received (VV); green is L-band vertically transmitted and horizontally received (VH); and blue is C-band (6 cm) VV. We add synthetic Gaussian noise of $\sigma = 20$ (figure 2a) to further challenge the scheme. Figure 1 (top row) shows the noisy channels and their corresponding denoised versions are given in figure 1 (bottom row). The final noisy and denoised multispectral images are shown in figure 2 (a) and (b) respectively. As can be seen from the results, apart from the better edge preservation, noise is removed, and the river boundary and farmlands with variety of colors representing crops surrounding it are also preserved.

To show the advantage of the coupling term we compare our proposed scheme (equation (2)) with the schemes of Acton and Landis (1997) (AL), Pope and Acton (1998) (PA), Lennon *et al.* (2002) (LMH), Wang *et al.* (2005) (WZL), the generalized spatio-chromatic diffusion scheme of Boccignone *et al.* (2002) (BFT) and Tschumperlé and Deriche (2005) (TD), and the vectorial TV of Bresson and Chan (2008) (BC) which were originally proposed for colour images and extended to the multispectral case. Figure 3 shows comparison results using a closeup of farmlands from the rectangular area indicated in figure 1(c). As can be seen by comparing figure 3(h) with other

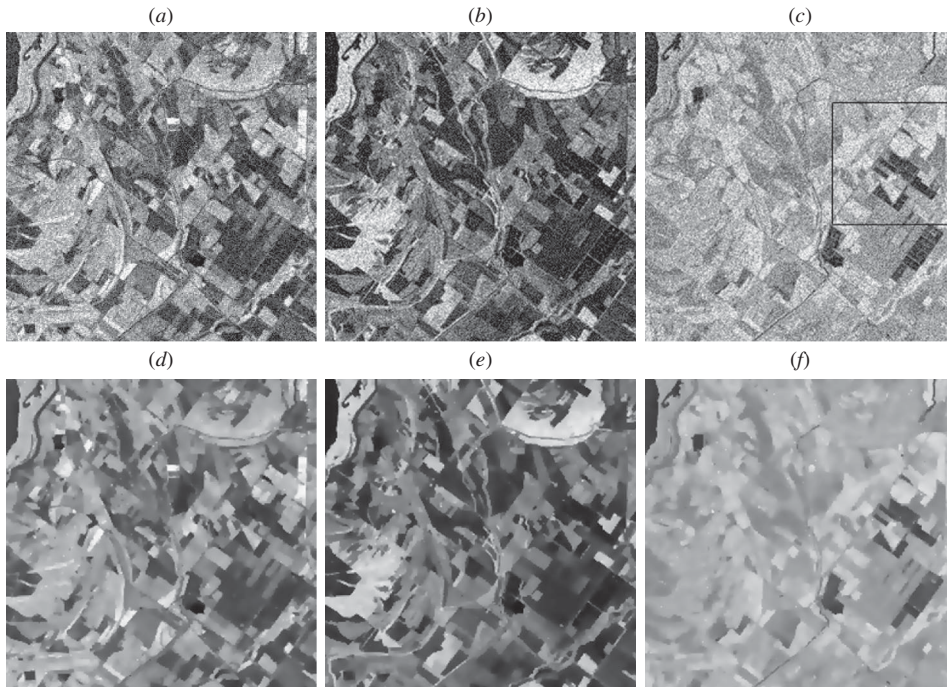


Figure 1. SIR-C in separate channels showing the effect of our scheme ($\alpha = 40$). Top row: noisy channels, bottom row: restored channels. (a) and (d) L-band VV; (b) and (e) L-band VH; (c) and (f) C-band VV. The extent of the area inside the rectangle in the upper right figure is shown in more detail in figure 3.

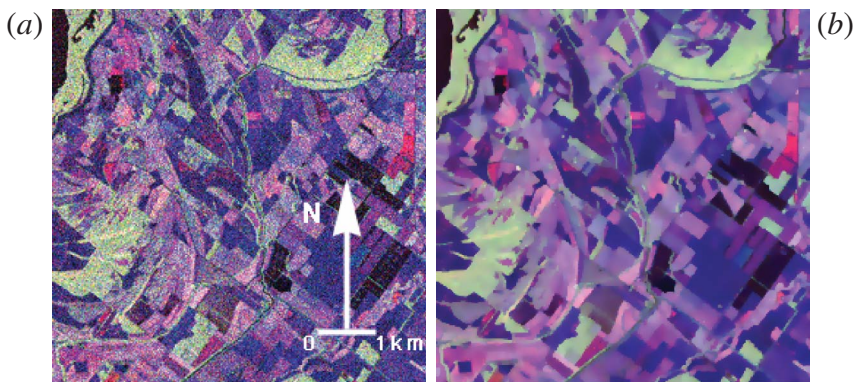


Figure 2. Multispectral L-band VV, L-band VH, and C-band VV on RGB image with added noise in each channel ($\sigma = 20$). (a) noisy combined image; (b) denoised image ($\rho = 2$, $t = 100$).

scheme's results, the proposed PDE avoids staircasing artifacts and other false color appearances due to incorrect channel mixing; moreover denoising respects the edges. Figure 3(i) depicts the coupling term in (R,G,B) for visualization, showing the multi-channel edges used in the diffusion PDE.

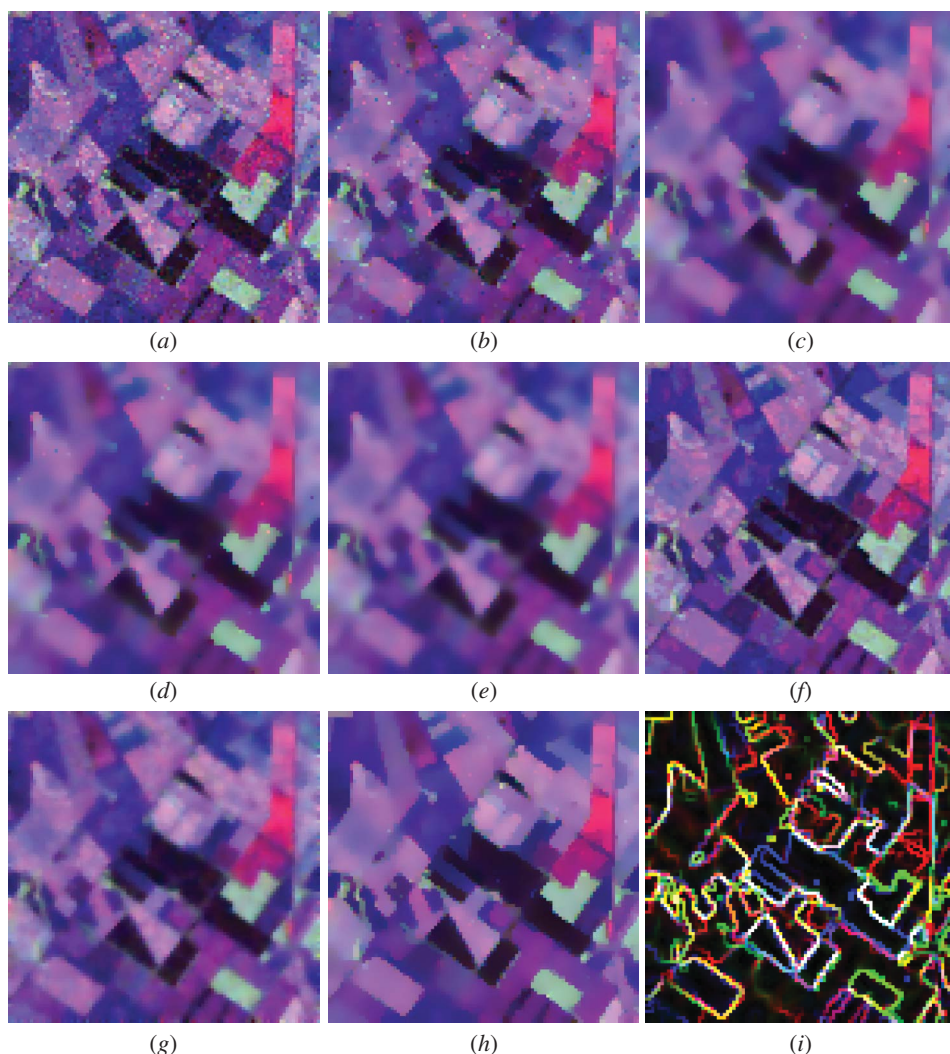


Figure 3. Comparison of results from the rectangular area indicated in figure 1. All images are false color composites of L-band VV, L-band VH, and C-band VV as RGB. (a) AL scheme; (b) PA scheme; (c) LMH scheme; (d) WZL scheme; (e) BFT scheme; (f) TD scheme; (g) BC scheme; (h) our scheme result. (i) The coupling term in the PDE (2) with weights computed using equation (3) shown here in RGB colors for visualization.

In the next example, a multispectral image of the south San Francisco bay area, shown in figure 4 (a), taken by the IRS-1C LISS-III sensor in four bands, i.e. 0.52–0.59, 0.62–0.68, 0.77–0.86 and 1.55–1.70 μm , on September 1999 (spatial resolution of the first three bands is 23.5 m, whereas for the fourth band, it is 70.5 m; the analysis and figure is based on the use of just the first three bands). We take the case of high noise $\sigma = 30$ and test our PDE given in equation (2) with updated weights from equation (5). As can be seen from figure 4 (b), the restored image consists of strong coherent edges and smoothed homogenous regions. In order to quantify the visual comparisons, the Peak Signal-to-Noise Ratio (PSNR) value is used as a measure of

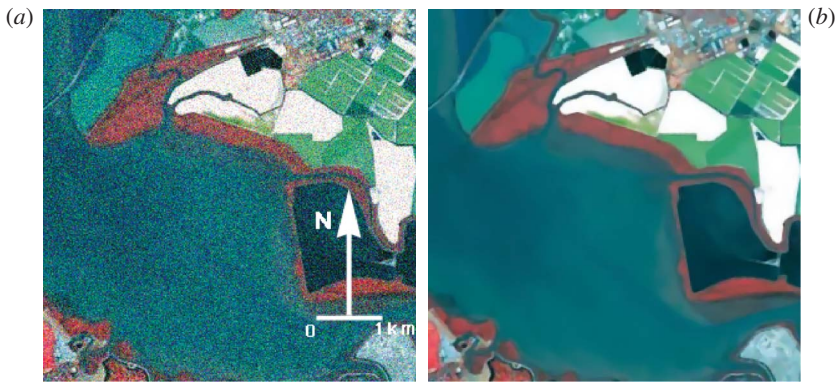


Figure 4. Multispectral image with high noise ($\sigma = 30$). (a) noisy image; (b) denoised image with adaptive weights (5) ($\rho = 3$, $t = 150$).

Table 1. Comparative peak signal-to-noise ratio PSNR (dB) results for various schemes; see §3 for the abbreviated names of schemes.

Image	σ	Noisy	AL	PA	LMH	WZL	BFT	TD	BC	Our
Figure 2	20	22.08	28.12	28.23	29.86	28.43	29.45	31.04	29.31	31.74
Figure 4	30	18.57	27.43	27.80	29.21	28.18	28.78	30.10	29.45	30.25

quality and it is given in table 1. For an estimated N-D image $\hat{\mathbf{u}}$, PSNR is given by $\text{PSNR}(\hat{\mathbf{u}}) = 10 \log((N \times \mathbf{u}_{\max}^2)/\text{MSE}) \text{ dB}$, where $\text{MSE} = \sum_{x \in \Omega} (\hat{\mathbf{u}}(x) - \mathbf{u}(x))^2 / |\Omega|$ is the mean squared error, $|\Omega|$ is the dimension of the image domain Ω , and \mathbf{u}_{\max} is the maximum value; for 8-bit images $\mathbf{u}_{\max} = 255$.

The effect of the denoising procedure in terms of smoothing image objects also depends on the parameters and time t in our scheme (equations (2)–(3)) apart from the presmoothing parameter ρ . The extent of image smoothing with respect to the selected set of parameters can be seen in figure 3(h). Moreover, figure 3(i) indicates an improvement with respect to edge detection and image segmentation for multichannel images when compared to the scheme of Karantzas and Argialas (2006). The stopping time t is related to the scale of choice, and when run for a longer time our scheme resulted in piecewise constant image separated by strong discontinuities. The weight balances the influence of interchannel edges and it can be tuned in terms of channel importance. A detailed analysis of parameter selection will further our knowledge and will be reported elsewhere.

We note that the computational complexity of the diffusion scheme depends on the number of channels in the input data. For $512 \times 512 \times 3$ size image our non-optimized finite difference scheme implementation takes about 1 min to denoise (100 iterations). Future directions to explore include extending the scheme to hyperspectral images (Lennon *et al.* 2002, Martín-Herrero 2007) and handling speckle (Han *et al.* 2002) or, in general, multiplicative noise models (Xu 1999) for multidimensional image denoising.

4. Conclusion

In this paper, denoising multispectral images using coupled partial differential equations with anisotropic diffusion is presented. A novel correlation term for capturing the interchannel coupling and preserving the main features among different channels is proposed. The scheme uses a total variation function for intrachannel smoothing to preserve within-channel edges. The weights in the coupling term are computed from the input image automatically acting as a road map for diffusion. Well-posedness of the scheme guarantees the stability. The corresponding gradient descent equation is implemented and numerical results indicate that the scheme preserves multi-edges. Comparisons with other related schemes are undertaken to show the improvement achieved by the proposed method. The scheme can be used as an efficient prefiltering method for multispectral images for removing noise and enhancing salient edges that might aid further processing.

Acknowledgements

We thank the anonymous reviewers and the editor, Dr. Timothy Warner, for their comments which greatly improved the content and presentation of the paper.

References

- ACTON, S.T. and LANDIS, J., 1997, Multi-spectral anisotropic diffusion. *International Journal of Remote Sensing*, **18**, pp. 2877–2886.
- AUBERT, G. and KORNPROBST, P., 2006, *Mathematical Image Processing: Calculus of Variations and Partial Differential Equations*, 2nd edition (New York: Springer-Verlag).
- BOCCIGNONE, G., FERRARO, M. and CAELLI, T., 2002, Generalized spatio-chromatic diffusion. *IEEE Transactions on Pattern Analysis and Machine Intelligence*, **24**, pp. 1298–1309.
- BRESSON, X. and CHAN, T.F., 2008, Fast dual minimization of the vectorial total variation norm and applications to color image processing. *Inverse Problems and Imaging*, **2**, pp. 455–484.
- BREZIS, H., 1973, *Opérateurs Maximaux Monotones et Semi-Groupes de Contractions dans les Espaces de Hilbert* (Amsterdam: North-Holland).
- CHAMBOLLE, A., 2004, An algorithm for total variation minimization and applications. *Journal of Mathematical Imaging and Vision*, **20**, pp. 89–97.
- GIUSTI, F., 1984, *Minimal Surfaces and Functions of Bounded Variation*, Monographs Math. Vol. 80 (Basel: Birkhäuser).
- HAN, C.M., GUO, H.D., WANG, C.L. and DIAN, F., 2002, A novel method to reduce speckle in SAR images. *International Journal of Remote Sensing*, **23**, pp. 5095–5101.
- IM, J., JENSEN, J. and TULLIS, J., 2008, Object-based change detection using correlation image analysis and image segmentation techniques. *International Journal of Remote Sensing*, **29**, pp. 399–423.
- KARANTZALOS, K. and ARGIALAS, D., 2006, Improving edge detection and watershed segmentation with anisotropic diffusion and morphological levelings. *International Journal of Remote Sensing*, **27**, pp. 5427–5434.
- LENNON, M., MERCIER, G. and HUBERT-MOY, L., 2002, Nonlinear filtering of hyperspectral images with anisotropic diffusion. In *Proceedings of the IEEE International Geoscience and Remote Sensing Symposium*, 25–29 July 2002, pp. 2477–2479.
- MARTÍN-HERRERO, J., 2007, Anisotropic diffusion in the hypercube. *IEEE Transactions on Geoscience and Remote Sensing*, **45**, pp. 1386–1398.
- PERONA, P. and MALIK, J., 1990, Scale-space and edge detection using anisotropic diffusion. *IEEE Transactions on Pattern Analysis and Machine Intelligence*, **12**, pp. 629–639.

- POPE, K. and ACTON, S.T., 1998, Modified mean curvature motion for multispectral anisotropic diffusion. In *Proceedings of the IEEE Southwest Symposium on Image Analysis and Interpretation*, 5–7 April 1998, Tucson, AZ, USA, pp. 154–159.
- RUDIN, L., OSHER, S. and FATEMI, E., 1992, Nonlinear total variation based noise removal algorithms. *Physica D*, **60**, pp. 259–268.
- SMOLKA, B. and LUKAC, R., 2002, On the combined forward and backward anisotropic diffusion scheme for the multispectral image enhancement. *The International Archives of the Photogrammetry, Remote Sensing and Spatial Information Sciences*, **34**, pp. 249–254.
- TSCHUMPERLÉ, D. and DERICHE, R., 2005, Vector-valued image regularization with PDE's: A common framework for different applications. *IEEE Transactions on Pattern Analysis and Machine Intelligence*, **27**, pp. 1–12.
- WANG, Y., ZHANG, L. and LI, P., 2005, Nonlinear multispectral anisotropic diffusion filters for remote sensed images based on MDL and morphology. In *Proceedings of the IEEE International Geoscience and Remote Sensing Symposium*, 25–29 July 2005, pp. 4327–4330.
- XU, P.L., 1999, Despeckling SAR-type multiplicative noise. *International Journal of Remote Sensing*, **20**, pp. 2577–2596.